ACS Chemical Neuroscience

pubs.acs.org/chemneuro

Research Article

Ruthenium-Mediated ^{18}F-Fluorination and Preclinical Evaluation of a New CB_1 Receptor Imaging Agent [^{18}F]FPATPP

Salla Lahdenpohja,▲ Noora A. Rajala,▲ Jatta S. Helin, Merja Haaparanta-Solin, Olof Solin, Francisco R. López-Picón, and Anna K. Kirjavainen*

Cite This: *ACS Chem. Neurosci.* 2020, 11, 2009−2018

Read Online

ACCESS | Metrics & More | Article Recommendations

ABSTRACT: Cannabinoid receptor 1 (CB1R) controls various physiological and pathological conditions, including memory, motivation, and inflammation, and is thus an interesting target for positron emission tomography (PET). Herein, we report a ruthenium-mediated radiolabeling synthesis and preclinical evaluation of a new CB1R specific radiotracer, [^{18}F]FPATPP. [^{18}F]FPATPP was produced with 16.7 ± 5.7% decay-corrected radiochemical yield and >95 GBq/μmol molar activity. The tracer showed high stability, low defluorination, and high specific binding to CB1Rs in mouse brain.

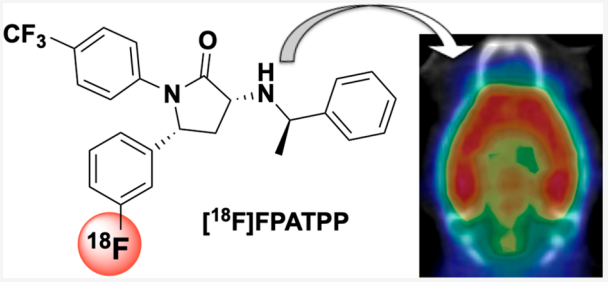

KEYWORDS: *Positron emission tomography, radiofluorination, fluorine-18, cannabinoid receptor, CB1R, FPATPP*

INTRODUCTION

Cannabinoid receptors, part of the endocannabinoid system, are expressed throughout the nervous system. Cannabinoid receptors are divided into two classes, cannabinoid receptor 1 (CB1R) and cannabinoid receptor 2 (CB2R). CB1R is a seven transmembrane domain G protein-coupled receptor (GPCR) and is one of the most abundant GPCRs in the brain.[1,2] In the brain, CB1Rs are localized, e.g., in cerebral cortex, especially the allocortex, basal ganglia and globus pallidus, substantia nigra, cerebellum, and medulla. Among vertebrate species, CB1Rs are highly conserved.[3,4] Until recently, unlike CB1Rs, the expression of CB2R in the CNS was thought to be very low.[1,2] However, recent studies have demonstrated the expression of the $CB2_A$ isoform in the brain. These receptors can be upregulated under pathological conditions.[5,6] In the periphery and the brain, CB1Rs are mainly found in presynaptic neurons where they inhibit release of neurotransmitters, e.g., γ-aminobutyric acid (GABA) and glutamate.[1,2] Activation of CB1Rs leads to activation of various signal transduction pathways, such as adenylyl cyclase regulation and ion channel regulation.[1] CB1Rs control various physiological and pathological conditions such as brain development, memory and learning, appetite, motivation, sensation of pain, and inflammation. This result is in agreement with the high CB1R concentration found in the sensory, cognition, and motor regions in the brain.[2] Alterations in the endocannabinoid system and CB1R expression can be caused by various neuropsychiatric and neurodegenerative conditions,[7] e.g., Alzheimer's disease (AD) impairs the CB1R activity.[8]

Positron emission tomography (PET) has been utilized to monitor CB1R expression in humans. Until this point, a few CB1R specific ^{11}C- or ^{18}F-labeled radioligands have been developed, such as (3*R*,5*R*)-5-(3-[^{11}C]methoxyphenyl)-3-[(*R*)-1-phenylethylamino]-1-(4-trifluoromethylphenyl) ([^{11}C]-MePPEP, [^{11}C]**1**),[9] (3*R*,5*R*)-5-(3-([^{18}F]fluoromethoxy)-phenyl)-3-(((*R*)-1-phenylethyl)amino)-1-(4-(trifluoromethyl)-phenyl)pyrrolidin-2-one ([^{18}F]FMPEP-d_2, [^{18}F]**2**),[10] and *N*-{(1*S*,2*S*)-2-(3-cyanophenyl)-3-[4-(2-[^{18}F]fluoroethoxy)-phenyl]-1-methylpropyl}-2-methyl-2-[(5-methylpyridin-2-yl)-oxy]propanamide ([^{18}F]MK-9470, [^{18}F]**3**, Figure 1).[11,12]

Fluorine-18 is an attractive radionuclide for PET applications due to its physical properties. Its relatively long half-life (109.8 min) enables even demanding synthesis and imaging protocols. The low positron energy (maximum ß$^+$ energy 635 keV) allows for high resolution imaging. In addition, aqueous [^{18}F]fluoride can be easily accessed with a cyclotron. However, the use of [^{18}F]fluoride in traditional nucleophilic labeling reactions, especially in the labeling of electron-rich structures, can be challenging. Late-stage ^{18}F-fluorination of arenes and heteroarenes with [^{18}F]fluoride has been widely studied, and various synthesis methods with various labeling precursors have been developed.[13−17] Metal-free approaches to ^{18}F-

Received: May 25, 2020
Accepted: June 1, 2020
Published: June 1, 2020

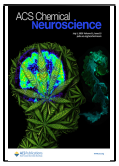

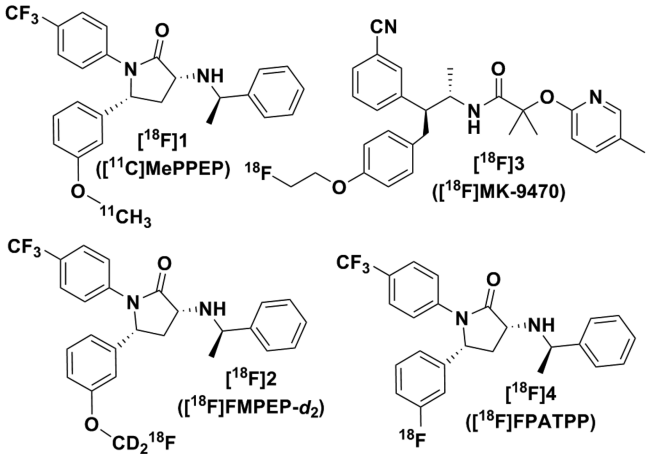

Figure 1. Chemical structures of [^{11}C]**1**, [^{18}F]**2**, [^{18}F]**3**, and [^{18}F]**4**.

fluorination utilize aryliodonium salts,[18] arylsulfonium salts,[19] and iodonium ylides[20] as precursors. Metal-mediated ^{18}F-fluorination utilizes complex Pd and Ni compounds as labeling precursors in the Pd-[21] and Ni-mediated[22] labeling processes, respectively. In Cu-mediated ^{18}F-fluorination, arylboronic esters,[23] arylboronic acids,[24] and arylstannanes[25] have been used as labeling precursors. Cu-mediated ^{18}F-labeling has gained wide popularity due to the straightforward synthesis, relatively easy access to precursor materials, and wide substrate scope. However, Cu-mediated labeling of compounds containing unprotected alcohols or amines can lead to undesired side reactions. Recently, a Ru-mediated ^{18}F-deoxyfluorination reaction *via* an *in situ* prepared η^6-coordinated ruthenium−phenol complex was introduced.[26] Ruthenium has been successfully applied in the ^{18}F-fluorination of small molecules containing electron-rich structures, including unprotected amines and heterocyclic scaffolds,[26] and in the site-specific ^{18}F-labeling of small peptides.[27] ^{18}F-Deoxyfluorination is an appealing method due to the use of easily accessible phenols as starting materials.

Recently, [^{18}F]FMPEP-d_2 has been widely used in CB1R PET studies, e.g., for imaging in schizophrenia and changes in CB1Rs in first-episode psychosis,[28] to study differences in brain CB1Rs between the sexes,[29] in brown adipose tissue,[30] and in AD.[31] An advantage of [^{18}F]FMPEP-d_2 is its high selectivity toward CB1Rs over CB2Rs, especially in regard to the ongoing discussion[5] of CB2R expression in the brain. A shortcoming of this tracer is its tendency toward radiolytic decomposition.[10,32] In this study, our objective was to utilize the ruthenium-mediated radiofluorination pathway to produce a stable CB1R specific tracer (3*R*,5*R*)-5-(3-[^{18}F]fluorophenyl)-3-(((*R*)-1-phenylethyl)amino)-1-(4-(trifluoromethyl)phenyl)-pyrrolidin-2-one ([^{18}F]FPATPP, [^{18}F]**4**, Figure 1), an analogue of [^{18}F]FMPEP-d_2, and to evaluate its usefulness for imaging *in vivo* and *ex vivo* with wild-type mice.

RESULTS AND DISCUSSION

Chemistry. We developed a simple route to produce a nonradioactive reference standard **4** for [^{18}F]**4**, following the original precursor synthesis,[10] as presented in Scheme 1. Briefly, compound **5** was produced from ethyl pyruvate, 4-aminobenzotrifluoride, and 3-methoxybenzaldehyde in acetic acid with 45% yield. Acid-catalyzed hydrolysis of **5** with hydrochloric acid and glacial acetic acid yielded compound **6**.

Scheme 1. Synthesis of the Reference Standard 4[a]

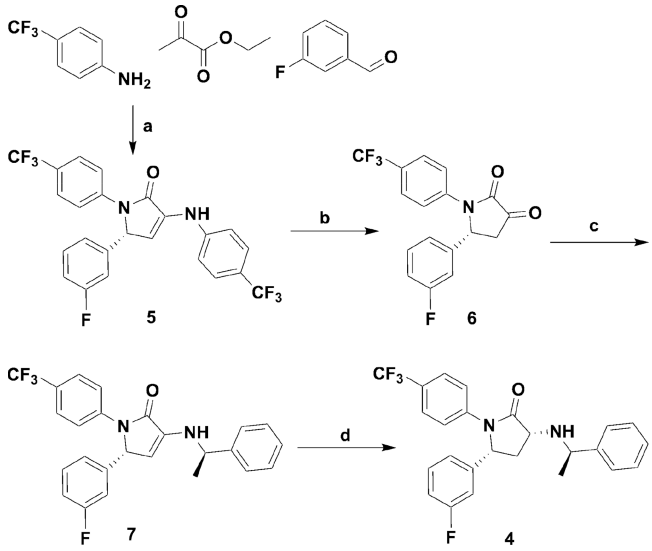

[a]Reagents and conditions: (a) acetic acid, (b) concentrated HCl and acetic acid, (c) (*R*)-(+)-1-phenylethylamine and CH_2Cl_2, and (d) $NaBH_3CN$ and acetic acid.

Compound **7** was separated from the mixture of isomers formed in the reaction with (*R*)-(+)-1-phenylethylamine and was further reduced with sodium cyanoborohydride to yield the reference standard **4**. The ruthenium complex, CpRu(COD)Cl was synthesized as previously reported[26] with a total synthesis yield of 20 ± 4% (n = 3)

Radiochemistry. We adapted a ruthenium-mediated labeling method[26] to produce [^{18}F]**4** starting from the phenol precursor **8**, CpRu(COD)Cl complex, and no-carrier added [^{18}F]fluoride (Figure 2A). *In situ* prepared ruthenium−phenol complex was used for the ^{18}F-radiolabeling reactions without purification. We performed an optimization study for the ^{18}F-radiofluorination reaction. The effect of the activation method for aqueous [^{18}F]fluoride on radiochemical yield (RCY) was studied by using solid-phase extraction (SPE) (bars 1−2, Figure 2B) and traditional azeotropic distillation (bar 4, Figure 2B). With the SPE method, the reaction temperature was varied from 100 to 130 °C (bar 1, Figure 2B) and further to 160 °C (bar 2, Figure 2B) with 10, 20, and 30 min reaction times. With the azeotropic distillation method, the reaction was conducted at 160 °C for 10−30 min (bar 4, Figure 2B). To study the effect of the base (potassium carbonate), we activated [^{18}F]fluoride with the SPE method, added potassium carbonate to the reaction mixture, and followed the reaction for 30 min at 160 °C (bar 3, Figure 2B).

In the SPE method, the ruthenium−phenol complex was used for the [^{18}F]fluoride elution from the anion exchange cartridge with 93 ± 5% elution efficiency (n = 12). Using 100 °C reaction temperature, no reaction occurred even after 30 min. Elevation of the temperature from 100 to 130 °C afforded a RCY (based on HPLC analysis of the crude product) of 20.9 ± 0.3% (n = 3) after 30 min reaction (bar 1, Figure 2B). Further elevation of the temperature to 160 °C provided 47.4 ± 3.5% (n = 3) RCY (based on HPLC analysis of the crude product) after 30 min reaction (bar 2, Figure 2B).

The reaction occurred faster when [^{18}F]fluoride was activated *via* azeotropic distillation compared to the activation with the SPE method. With azeotropic distillation activation

https://dx.doi.org/10.1021/acschemneuro.0c00313
ACS Chem. Neurosci. 2020, 11, 2009−2018

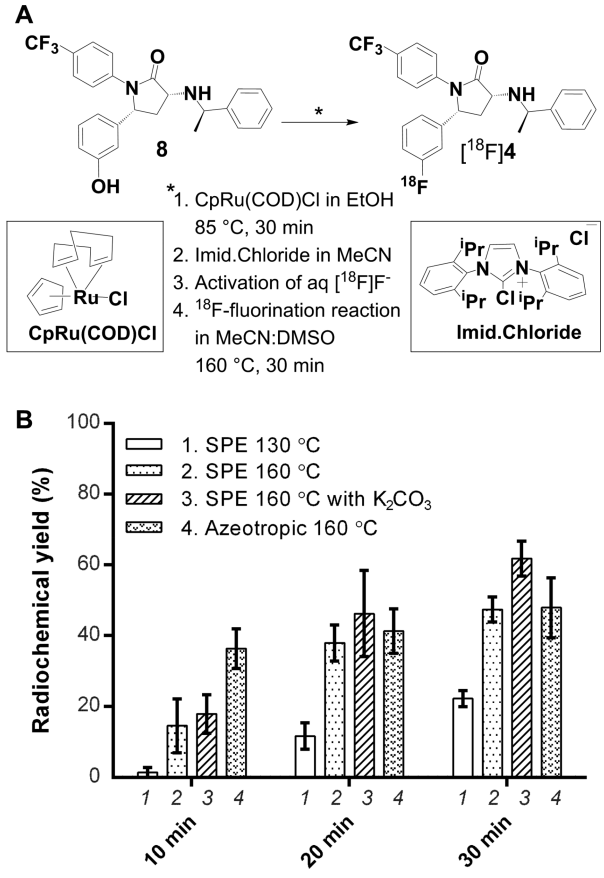

Figure 2. (A) Synthesis of [^{18}F]**4**. (B) Results from the process optimization. SPE + temperature denotes the solid-phase extraction with subsequent reaction temperature. Azeotropic + temperature denotes the traditional drying procedure of [^{18}F]fluoride with subsequent reaction temperature. Data are expressed as mean ± standard deviation (SD, n = 3).

(bar 4, Figure 2B), the RCY was already 36.3 ± 5.6% after a 10 min reaction and 47.9 ± 8.5% after a 30 min reaction (values based on HPLC analysis of the crude product) at 160 °C. Even though some of the initial [^{18}F]fluoride was lost during the azeotropic drying process *via* adherence to the glass vial, the RCY was considerably higher (36 vs 16%) after a 10 min reaction at elevated temperature compared to the SPE method.

The reaction mixture is more basic when using the azeotropic distillation method due to the addition of potassium carbonate. The effect of the additional base was further studied with the SPE method (bar 3, Figure 2B); the RCY was 17.9 ± 5.5% (n = 3) after a 10 min reaction time and 61.8 ± 4.9% (n = 3) after a 30 min reaction time. Thus, the addition of a base improved the RCY by ∼30% with a 30 min reaction.

For tracer production for preclinical evaluation, larger amounts of initial [^{18}F]fluoride were used and full purification and formulation processes were performed. For the radiofluorination, the SPE method with a 30 min reaction at 160 °C was utilized (conditions as in bar 2, Figure 2B). Elution efficiency was 93 ± 2% (n = 5). Total RCY was 16.7 ± 5.7% (decay-corrected to end of bombardment, d.c. to EOB, n = 5), molar activity (A_m) > 95 GBq/μmol (d.c. to end of synthesis, EOS, n = 1) and radiochemical purity (RCP) 99.9 ± 0.1% at EOS (n = 5). Activity yield was 1.0 ± 0.4 GBq (n = 5) at EOS. Synthesis time was 87 ± 5 min (n = 5). The amount of ruthenium in the formulated product was 7.8 ± 1.8 μg/mL. Stability of [^{18}F]**4** was studied up to 5 h after the EOS, and no significant decomposition was observed (n = 2).

For PET applications, late-stage fluorination approaches are highly desirable to minimize the radiosynthesis time and to avoid the multiple purification processes often needed in multistep radiosyntheses. Ruthenium-mediated ^{18}F-fluorination starting from a phenol precursor is a facile labeling method with reasonable synthesis time and good RCY. The present optimized reaction conditions, 30 min at 160 °C, were even harsher than typical reaction conditions of traditional nucleophilic ^{18}F-fluorination. However, the good RCY and robustness of the present conditions (bar 3, Figure 2B), demonstrated by the low SD, are advantageous. For potential clinical applications, the ruthenium content in the formulated preparation must be considered. The maximum parenteral daily exposure of ruthenium according to ICH Q3D(R1) is limited to 10 μg/day.[33] In this material, the ruthenium content is rather high, limiting the administrable volume of [^{18}F]**4**. Thus, the purification process needs to be refined in order to reduce the ruthenium content before clinical tracer production can be conducted *via* ruthenium-mediated ^{18}F-labeling.

For PET tracers for clinical use, a generally acknowledged limit for RCP is 95%. A significant difference was found in the RCP at EOS and stability of [^{18}F]**4** compared to [^{18}F]FMPEP-d_2. Lahdenpohja et al. reported that the RCP of [^{18}F]FMPEP-d_2 at EOS varied between 95.5−100% and was a function of radioactivity concentration, which was 20−200 MBq/mL (n > 150) in a 10% ethanolic solution, and the RCP was declined as a function of time due to radiolytic decomposition.[32] The shelf life of the [^{18}F]FMPEP-d_2 was determined to be 120 min.[32] For [^{18}F]**4** formulated in a similar ethanolic solution, the RCP at EOS was 99.9% when the RAC was 200−450 MBq/mL and the shelf life was determined to be at least 300 min, with no significant development of radioactive impurities. This difference in stability toward radiolysis is an advantage of [^{18}F]**4** as compared to [^{18}F]FMPEP-d_2.

Animal Studies. The animal studies were divided into five sections; *in vivo* 120 min dynamic PET/computed tomography (CT) studies, *ex vivo* digital autoradiography of brain at 120 min, *ex vivo* biodistribution at 30, 60, and 120 min, and radiometabolite analysis at 30, 60, and 120 min. The fifth separate section was an *ex vivo* biodistribution study with [^{18}F]FMPEP-d_2. The potency and receptor selectivity of [^{18}F]**4** was not determined separately. However, blocking studies using the selective CB1R antagonist rimonabant (SR141716) were conducted for both *in vivo* PET and *ex vivo* autoradiography and biodistribution. Rimonabant is highly specific for CB1Rs in the CNS (K_i 1.98 nM), and its selectivity for CB1Rs over CB2Rs is more than 1000 fold.[34] Rimonabant is thus suitable to demonstrate the specificity of the tracer to CB1Rs.

***In Vivo* PET Imaging.** *In vivo* evaluation was performed for [^{18}F]**4** with wild-type mice with (n = 3, 1 female) and without blocking (n = 3, 1 female). The [^{18}F]**4** tracer uptake reached its maximum 30 min after the injection. This observation is comparable to a mice study by Takkinen et al. with [^{18}F]FMPEP-d_2, which similarly reached its tracer uptake maximum at 30 min.[31] In a rat study by Casteels et al. with [^{18}F]MK-9470, the tracer uptake was considerably slower, reaching its maximum at 300 min post injection (p.i.).[11] The peak standardized uptake values (SUVs) of [^{18}F]**4** were 1.92 for the whole brain, 1.80 for the neocortex, and 2.14 for the hippocampus (Figure 3A−D). This outcome is somewhat

https://dx.doi.org/10.1021/acschemneuro.0c00313
ACS Chem. Neurosci. 2020, 11, 2009−2018

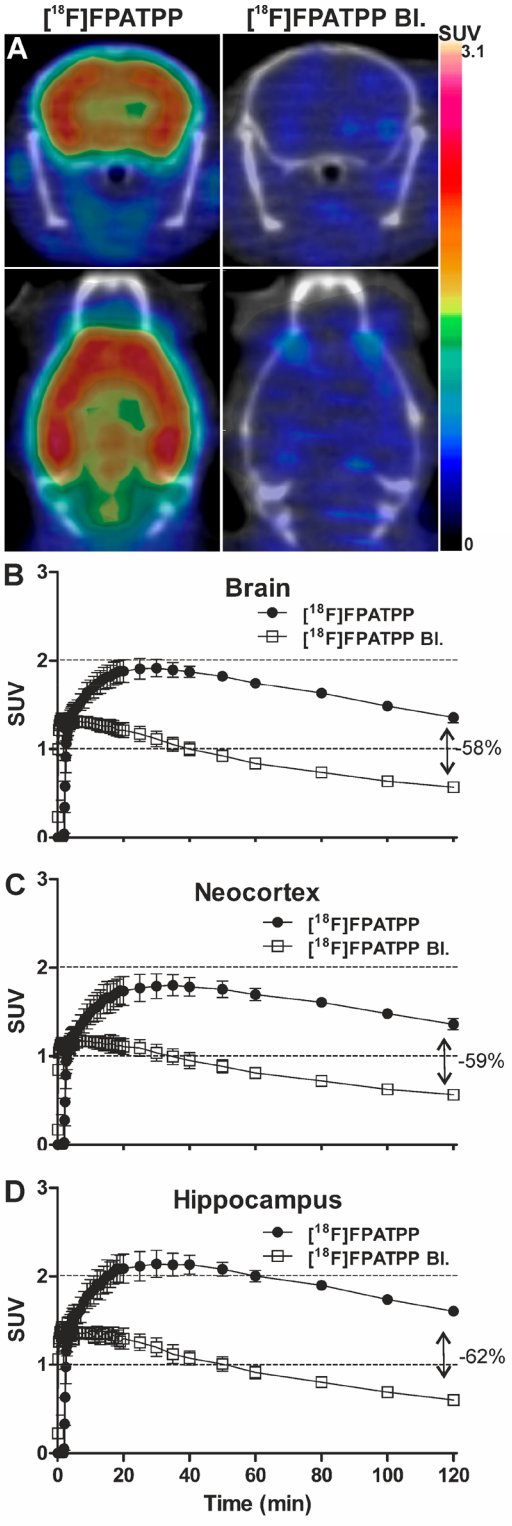

Figure 3. (A) Representative coronal and transaxial [^{18}F]**4** PET/CT images summed for 90−120 min in an adult mouse brain with vehicle (left) and 2 mg/kg rimonabant pretreatment (right). (B−D) Time−activity curves for the whole brain, neocortex, and hippocampus at baseline (n = 3, 1 female) and with rimonabant pretreatment (n = 3, 1 female) and their percentage difference at 120 min. Bl., Blocking; SUV, standardized uptake value. Data are expressed as mean ± SD.

higher than with [^{18}F]FMPEP-d_2, where the whole brain SUV was 1.5,[31] and noticeably higher than with [^{18}F]MK-9470, where the whole brain SUVs were 0.6−1.6 in rats.[11] For [^{18}F]**4**, the washout phase began immediately after the peak uptake, declining to a SUV of 1.3 at 120 min p.i. For [^{18}F]FMPEP-d_2, essentially no washout was observed up to 90 min p.i. in the study by Takkinen et al.[31] For [^{18}F]MK-9470, no washout was observed even after 600 min in the study with rats by Casteels et al.[11] Human studies using [^{18}F]FMPEP-d_2 demonstrated slow washout,[35] and with [^{18}F]MK-9470, no washout was observed even after 6 h.[36] Overall, the uptake behavior and the kinetics suggest that [^{18}F]**4** might show superior characteristics in clinical imaging compared to [^{18}F]FMPEP-d_2 and [^{18}F]MK-9470.

The pretreatment with 2 mg/kg rimonabant reduced the binding of [^{18}F]**4** 120 min after injection by 58, 59, and 62% for the whole brain, neocortex, and hippocampus, respectively (Figure 3A−D), when the injected amount of [^{18}F]**4** was 1.7 ± 0.7 μg/kg (n = 6). The moderate dose of rimonabant blocked a large percentage of the binding of [^{18}F]**4** in specific murine CB1R-rich areas, such as the neocortex and hippocampus, and avoided CB1R poor areas, such as the thalamus.

***Ex Vivo* Autoradiography.** In addition to the *in vivo* PET studies, we performed *ex vivo* brain autoradiographic studies 120 min after [^{18}F]**4** injection to examine smaller brain areas in more detail. Figure 4A shows specific [^{18}F]**4** binding in CB1R-rich areas, like striatum, globus pallidus, hippocampus, cortex, and cerebellar gray matter. The binding of [^{18}F]**4** even allowed us to distinguish different hippocampal and cortical layers and the cerebellar gray matter with similar resolution to the *in vitro* studies in mice using the CB1R agonist [^{3}H]CP55,940[37,38] or showing similar hippocampal distribution to that observed in CB1R immunohistochemical studies.[39] Previous autoradiography studies in mice with the PET radioligand [^{18}F]FMPEP-d_2 did not discriminate the cortical and hippocampal layering with as high a resolution.[31]

The blocking of [^{18}F]**4** with rimonabant was also evident in the autoradiographic images (Figure 4A). In addition, we quantified the binding of [^{18}F]**4** in the different CB1R-rich regions using the thalamus as a reference region given the very low level of CB1Rs in that brain region in mice (Figure 4B). The ratios with respect to the thalamus were 2.3 for the parietotemporal cortex, 2.8 for the striatum, 2.5 for the frontal cortex, 2.6 for the whole hippocampus, 3.7 for the cortex and cerebellar gray matter, and 4.9 for the globus pallidus. The region-to-thalamus ratios in the mice pretreated with rimonabant were close to 1, indicating complete displacement of specific tracer binding. The P values were less than 0.001 for all analyzed regions.

Biodistribution. We evaluated [^{18}F]**4** biodistribution at 30, 60, and 120 min p.i. (Figure 5A). We observed high ^{18}F-radioactivity binding in the whole brain, cortex, and liver. The whole brain uptake was 9.8 ± 3.2% of the injected dose per gram of tissue (%ID/g), the cortex uptake was 11.5 ± 3.7%ID/g, and the liver uptake was 12.1 ± 0.7%ID/g at 30 min p.i. Radioactivity washout was moderate; hence, the measured whole brain uptake was 4.9 ± 0.9%ID/g, the cortex uptake was 5.1 ± 1.17% ID/g, and the liver uptake was 8.2 ± 1.6%ID/g at 120 min p.i. Bone uptake at 120 min p.i. was insignificant (0.4 ± 0.1%ID/g), indicating a low defluorination and subsequent bone accumulation. In the rimonabant treated mice, the cortex uptake at 120 min p.i. was 1.8 ± 0.2%ID/g.

In a separate study, we investigated the *ex vivo* biodistribution of [^{18}F]FMPEP-d_2 in healthy mice (Figure 5B). It is worth noting that [^{18}F]FMPEP-d_2 had lower ^{18}F-

https://dx.doi.org/10.1021/acschemneuro.0c00313
ACS Chem. Neurosci. 2020, 11, 2009−2018

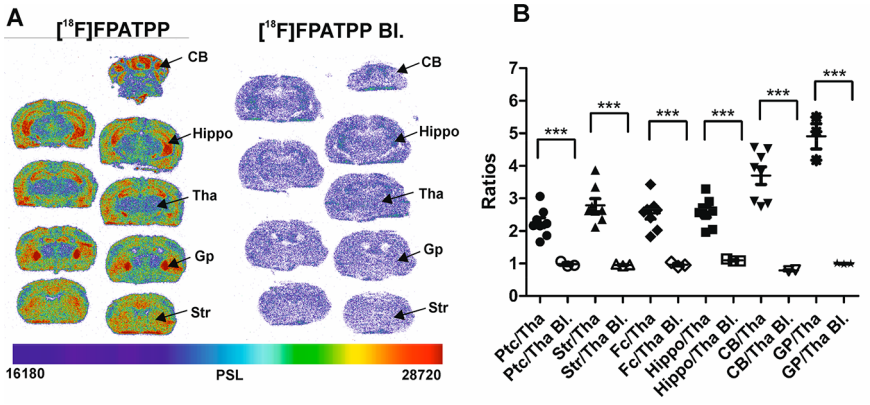

Figure 4. (A) Representative *ex vivo* brain autoradiography images of [^{18}F]**4** binding 120 min post injection in a nontreated mouse and a mouse pretreated with rimonabant to block the [^{18}F]**4** binding. (B) Ratios of the parietotemporal cortex (Ptc), striatum (Str), frontal cortex (Fc), hippocampus (Hippo), cortex, cerebellar gray matter (CB), and globus pallidus (Gp, n = 3, 1 female) to the thalamus (Tha) without blocking (n = 8, 1 female) and with blocking (Bl. n = 3, 1 female). ***P < 0.001, statistical analyses were performed with the Mann–Whitney U test.

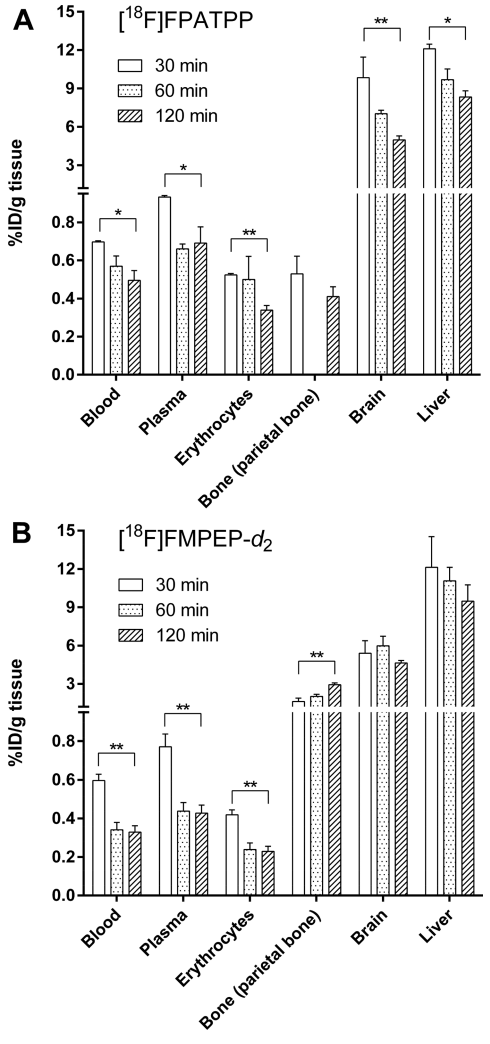

Figure 5. *Ex vivo* biodistribution of (A) [^{18}F]**4** (30 min n = 4, 60 min n = 2, 120 min n = 8, 1 female) and (B) [^{18}F]FMPEP-d_2 (30 min n = 3, 60 min n = 4, 120 min n = 12, 5 females). Data are presented as injected dose per gram of tissue (%ID/g) and expressed as mean ± SD. *P < 0.05, **P < 0.005, statistical analyses were performed with the Mann–Whitney U test.

radioactivity uptake, 5.6 ± 1.3%ID/g, in the whole brain at 30 min p.i. than with [^{18}F]**4**. In addition, skull bone (parietal bone) radioactivity uptake showed a great difference; with [^{18}F]FMPEP-d_2, uptake was as high as 2.7 ± 0.5%ID/g at 120 min p.i. as compared to 0.4 ± 0.1%ID/g with [^{18}F]**4**. Defluorination of [^{18}F]FMPEP-d_2 at 120 min was over 6-fold compared to [^{18}F]**4**. In human studies, [^{18}F]FMPEP-d_2 defluorination has been low.[35] However, defluorination can lead to a high skull bone uptake and thus may obscure the imaging of close by structures due to the spillover effect. This result indicates that the ^{18}F-label located on the aromatic ring in [^{18}F]**4** is more stable against defluorination than the ^{18}F-label located in the [^{18}F]fluoromethoxy tail in [^{18}F]FMPEP-d_2.

Metabolite Analysis. [^{18}F]**4** was metabolized slowly. In the plasma and cortex samples collected at 120 min p.i. (n = 5), two polar radioactive metabolites in plasma and one in cortex were observed. The amount of residual [^{18}F]**4** in plasma was approximately 21.3 ± 3.5% of the total ^{18}F-radioactivity at 120 min p.i. The amount of residual [^{18}F]**4** in the cortex at 120 min p.i. was 75.0 ± 4.3% (Figure 6). The amount of residual [^{18}F]FMPEP-d_2 has been shown to be 86% at 180 min p.i., which is somewhat higher than the value obtained with [^{18}F]**4**.[31] However, the higher brain uptake of [^{18}F]**4** and much lower formation of [^{18}F]fluoride as compared to [^{18}F]FMPEP-d_2 will presumably be an advantage for imaging.

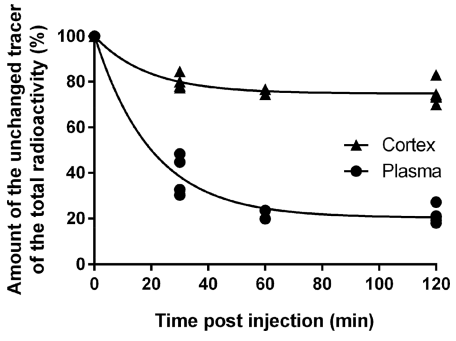

Figure 6. Amount of the [^{18}F]**4** of the total ^{18}F-radioactivity in plasma and cortex. The radiometabolites were analyzed at 30 min (n = 4), 60 min (n = 2), and 120 min (n = 5) post injection. A double exponential decay equation has been used for the fitting of the curves.

https://dx.doi.org/10.1021/acschemneuro.0c00313
ACS Chem. Neurosci. 2020, 11, 2009–2018

Summary of [^{18}F]4 Specificity and Selectivity. *In vivo* PET, *ex vivo* autoradiography, and *ex vivo* biodistribution blocking study results with the CB1R selective and specific rimonabant demonstrated specific receptor occupancy of [^{18}F]**4**. In addition, [^{18}F]**4** is a very close structural analogue to the well-known CB1R tracer [^{18}F]FMPEP-d_2, which has an *in vitro* potency (K_b) of 0.187 nM for CB1R and CB1R vs CB2R selectivity of 3580.[8] These observations support our conclusion that [^{18}F]**4** binds specifically to CB1Rs.

CONCLUSIONS

We successfully implemented a ruthenium-mediated late-stage radiofluorination method to produce a new CB1R imaging tracer, [^{18}F]FPATPP, [^{18}F]**4**. ^{18}F-labeling of the aromatic ring was effective with good RCY and reasonable synthesis time. There is room for improvement as the reaction conditions are harsh. Nonetheless, this proof-of-concept study shows that ruthenium-mediated ^{18}F-labeling is a suitable and robust method for radiotracer production. [^{18}F]**4** was shown to be more stable against radiolysis than its analogue [^{18}F]FMPEP-d_2 with an over 300 min shelf life compared to a 120 min shelf life. In the preclinical evaluation, [^{18}F]**4** showed significantly lower defluorination and faster washout compared to [^{18}F]-FMPEP-d_2. The *in vivo* and *ex vivo* results suggest that [^{18}F]**4** is a potent and selective tracer for CB1R. The properties of [^{18}F]**4** make the tracer suitable for clinical evaluation.

METHODS

Chemistry. *General Chemistry Methods.* FPATPP precursor, (3*R*,5*R*)-5-(3-hydroxyphenyl)-3-(((*R*)-1-phenylethyl)amino)-1-(4-(trifluoromethyl)phenyl)pyrrolidin-2-one, was obtained from PharmaSynth (PharmaSynth AS, Tartu, Estonia). The ruthenium complex was synthesized as previously published.[26] Reference standard **4** was synthesized, and the stereochemistry was assigned following the original precursor synthesis developed by Donohue et al.[10] All other reagents and solvents were purchased from commercial suppliers and were used as received.

Chromatographic Methods. NMR analyses were performed with a 500 MHz Bruker AVANCE-III NMR-system. The multiplicities are abbreviated as follows: s = singlet, d = doublet, t = triplet, m = multiplet, br = broad signal, dd = doublet of doublets, etc. MS analyses were performed with a linear ion trap quadrupole mass spectrometer (QTRAP, Applied Biosystems SCIEX) equipped with a Turbo Ion Spray source. Purity of the reference standard **4** was determined with HPLC. Ruthenium content in the final preparation was analyzed with inductively coupled plasma mass spectrometry (ICP-MS; PerkinElmer, Elan DRC Plus). Commercial standards were used for instrument calibration.

5-(3-Fluorophenyl)-1-(4-trifluoromethylphenyl)-3-(4-trifluoromethylphenylamino)-1,5-dihydropyr-rol-2-one (5). 4-Aminobenzotrifluoride (39.0 mL, 310.4 mmol) in glacial acetic acid (92 mL) was added to a solution of 3-methoxybenzaldehyde (11.0 mL, 103.5 mmol). Then, ethyl pyruvate (11.5 mL, 103 mmol) was added. The mixture was stirred at room temperature for 18 h. The precipitate was filtered and washed with a mixture of 20% MTBE in heptane (300 mL) and was dried under a vacuum to afford **5** (27.3 g, 45%) as an off-white powder. ^{1}H NMR ($CDCl_3$): δ 7.74 (d, J = 8.6 Hz, 2H), 7.68 (d, J = 8.9 Hz, 1H), 7.58 (d, J = 8.5 Hz, 2H), 7.57 (d, J = 8.5 Hz, 2H), 7.28 (CDCl3), 7.30−7.36 (m, 1H), 7.15 (d, J = 8.6 Hz, 2H), 6.99 (dt, J = 8.5 Hz, 2.2 Hz, 1H), 6.92 (td, J = 9.3 Hz, 1.9 Hz, 1H), 6.20 (d, J = 2.7, 1H), 5.76 (d, J = 2.6 Hz, 1H), 2.82 (br) ppm. ^{13}C NMR ($CDCl_3$): δ 143.8, 131.1, 126.8 (d), 126.3 (d), 122.2 (d), 120.5, 122.4, 120.5, 120.4, 119.3, 116.2, 113.5, 113.3, 112.9, 109.8, 90.7, 63.4 (d), 40.1, 39.9, 39.8 ppm. m/z: [M − H]$^-$. Calcd for $C_{24}H_{16}F_7N_2O$: 479.10. Found: 479.0.

5-(3-Fluorophenyl)-1-(4-trifluoromethylphenyl)-pyrrolidine-2,3-dione (6). A mixture of **5** (27.3 g, 273.5 mmol), glacial acetic acid (122 mL), and concentrated HCl (152 mL) was stirred at room temperature for 22 h. The heterogeneous solution was heated at 60 °C for 1 h. The mixture was poured onto ice (1 L), stirred, and let to stand for 1 h. The precipitate was filtered, washed with water, and dried under a vacuum overnight to afford a solid **6**. ^{1}H NMR (DMSO-d_6): δ 10.33 (br), 8.75 (s, 1H), 7.89 (d, J = 8.6 Hz, 2H), 7.82 (d, J = 8.6 Hz, 2H), 7.72 (d, J = 8.6 Hz, 2H), 7.67 (d, J = 8.7 Hz, 2H), 7.58 (d, J = 8.7 Hz, 2H), 7.47 (d, J = 8.6 Hz, 2H), 7.05−7.08 (m, 2H), 6.63 (d, J = 2.7 Hz, 1H), 6.24 (d, J = 2.7 Hz, 1H), 6.02 (d, J = 2.6 Hz, 1H), 6.01 (d, J = 2.6 Hz, 1H), 5.81 (dd, J = 7.5, 4.1 Hz, 1H), 3.37 (m, 1H), 2.62 (dd, J = 19.4, 4.1 Hz, 1H) ppm. m/z: [M + CHOO]$^-$. Calcd for $C_{18}H_{12}F_4NO_4$: 382.07. Found: 382.0.

(R)-5-(3-Fluorophenyl)-3-[(R)-1-phenylethylamino]-1-(4-trifluoromethylphenyl)-1,5-dihydropyrrol-2-one (7). (*R*)-(+)-1-Phenylethylamine (5.28 mL, 46 mmol) was added to a solution of **6** (8 g, 23 mmol) in CH_2Cl_2 (58 mL). The solution was stirred at room temperature for 18 h. A silica gel column was prepared in hexane. The solution was evaporated to dryness and dissolved with a small volume of EtOAc and was then poured onto a silica gel column. The material was purified by silica gel chromatography (5−15% EtOAc/hexane) to afford **7**, the second eluting isomer, as a yellow foam (2.8 g, 28%). ^{1}H NMR (DMSO-d_6): δ 7.89 (d, J = 8.7 Hz, 1H), 7.80 (d, J = 8.6 Hz, 2H), 7.72 (d, J = 8.8 Hz, 1H), 7.65 (d, J = 8.8 Hz, 2H), 7.58 (d, J = 8.8 Hz, 1H), 7.48 (d, J = 8.7 Hz, 1H), 7.34 to 7.38 (m, 2H), 7.26 (t, J = 7.6 Hz, 2H), 6.94 (dt, J = 8.6 Hz, 2.4 Hz, 1H), 6.86 (d, J = 7.8 Hz, 1H), 5.89−5.94 (m, 2H), 5.20 d, J = 2.6 Hz, 1H), 5.19 (quint, J = 2.6 Hz, 1H), 1.46 (d, J = 6.8 Hz, 3H) ppm. m/z: [M + H]. Calcd for $C_{25}H_{21}F_4N_2O$: 441.16. Found: 441.2.

(3R,5R)-5-(3-Fluorophenyl)-3-[(R)-1-phenylethylamino]-1-(4-trifluoromethylphenyl)-pyrrolidin-2-one (4). Compound **7** (2.8 g, 64 mmol) was dissolved in glacial acetic acid (31 mL), and sodium cyanoborohydride was added (800 mg, 12.4 mmol). The reaction mixture was stirred at room temperature for 1 h and concentrated *in vacuo*. The residue was dissolved in EtOAc and washed with a saturated $NaHCO_3$ solution, water, and brine. The organic layer was dried with Na_2SO_4 and concentrated *in vacuo*. Approximately a fourth of the product was dissolved in a small amount of EtOAc and purified by silica gel chromatography (10−30% EtOAc/hexane) to afford **4**, (the first eluting isomer) as a white solid (0.294 g, 10.4%). ^{1}H NMR (DMSO-d_6): δ 7.66 (d, J = 8.8 Hz, 2 H), 7.62 (d, J = 8.8 Hz, 2H), 7.42 (d, J = 8.7 Hz, 2H), 7.33−7.39 (m, 2H), 7.19−7.25 (m, 2H), 7.04 (dt, J = 8.4 Hz, 2.4 Hz, 1H), 6.86 (d, J = 8.7 Hz, 2 H), 5.5 (dd, J = 9.2 Hz, 6.7 Hz, 1H), 4.75 (td, J = 10.7 Hz, 8.4 Hz, 2.3 Hz, 1H), 3.41−3.48 (m, 1H), 3.05−3.14 (m, 1H), 1.77−1.87 (m, 1H), 1.31 (d, 3H) ppm. m/z: [M + H]. Calcd for $C_{25}H_{23}F_4N_2O$: 443.17. Found: 443.1. Purity (HPLC): 98.0%.

Radiochemistry. *General Radiochemistry Methods.* RCYs are decay-corrected to the start of the synthesis, which in this case corresponds to EOB. The RCYs (based on HPLC analysis) are based on the overall radioactivity eluted from the HPLC column, whereas the product fraction was collected in a separate vial. We determined that there was no leftover radioactivity in the injector or in the HPLC column after the analytical HPLC run. A_m calculation is decay-corrected to EOS. The concentration of the **4** in the formulated solution was low, below the detection limit of the UV-detector. Thus, the A_m value is based on the radioactivity collected at the analytical HPLC column outlet and the detection limit for the reference compound **4** (1 μg/mL).

Radio-Chromatographic Methods. Semipreparative HPLC purification of [^{18}F]FPATPP was conducted with a Jasco PU-2089 HPLC-pump (Jasco Inc., Easton, Maryland). A Luna C18 column (10 μm, 10.0 mm × 250 mm; Phenomenex, Milford, Massachusetts) and an isocratic method was used as follows: 57/43 1% TFA in H_2O/CH_3CN + ascorbic acid (500 mg/L). The flow rate was 8.0 mL/min, and detector λ = 254 nm. Analytical radio-HPLC was carried out with a VWR Hitachi L-2130 HPLC pump (VWR Hitachi, VWR International GmbH, Darmstadt, Germany) equipped with a VWR Hitachi L-2400 UV absorption detector and a 2 × 2 in.^{2} NaI radioactivity detector. A Luna C5 column (5 μm, 4.6 mm × 150 mm; Phenomenex) was used with following isocratic elution method: 55/

https://dx.doi.org/10.1021/acschemneuro.0c00313
ACS Chem. Neurosci. 2020, 11, 2009−2018

45 0.1% TFA in H_2O/CH_3CN. The flow rate was 0.95 mL/min, and detector λ = 254 nm.

[^{18}F]Fluoride Production. [^{18}F]F^- (aq) was produced by irradiating enriched Oxygen-18 water (GMP-grade, 98%, Rotem Industries Ltd., Medical Imaging, Dimona, Israel) with 17 MeV protons and a 40 μA beam current. The initial amount of [^{18}F]F^- used was 10.7 ± 3.3 GBq for preclinical studies and 1.15 ± 0.95 GBq for radiochemistry optimization studies.

Preparation of FPATPP Precursor for Radiosynthesis. FPATPP precursor (6.9 ± 0.7 μmol) and ruthenium complex (24.5 ± 2.5 μmol) were dissolved in ethanol (50 μL) and heated at 80 °C for 30 min. 1,3-*Bis*(2,6-diisopropylphenyl)imidazolium chloride was dissolved in MeCN (150 μL) and added to the reaction mixture to produce mixture **A**. The reaction mixture was used without purification.

Radiochemistry Optimization Study. Prior to the production of [^{18}F]FPATPP for preclinical studies, the Ru-mediated radiofluorination method was tested with temperatures from 100 to 160 °C and reaction times from 10 to 30 min. In addition, for drying of [^{18}F]fluoride, a SPE method and an azeotropic distillation method were tested.

In the SPE method, a PS-HCO_3^- anion exchange cartridge (Synthra GmbH, Hamburg, Germany) was used. Aqueous [^{18}F]F^- was trapped in a cartridge preconditioned with potassium oxalate (3 mL, 10 mg/mL) and water (2 mL). The cartridge was washed with CH_3CN (1 mL), and [^{18}F]F^- was eluted to a conical vial with mixture **A**. The cartridge was rinsed with DMSO (150 μL) and 1:1 DMSO/MeCN solution (50 μL). The reaction mixture was heated at 100, 130, or 160 °C for 30 min, and the reaction was followed with radio-HPLC. In the base-added SPE method, K_2CO_3 (40 μL, 14.8 ± 4.2 μmol, 45 mg/mL) was added to DMSO (150 μL) used for cartridge rinsing after [^{18}F]fluoride elution. The reaction mixture was heated at 160 °C for 30 min, and the reaction was followed with radio-HPLC.

In the azeotropic distillation method, aqueous [^{18}F]F^- solution was dried using azeotropic distillation with MeCN, K_2CO_3 (14.8 ± 4.2 μmol), and Kryptofix K_{222} (16.6 ± 0.6 μmol) at 120 °C with helium flow to form the dry [^{18}F]KF/K_{222}-complex. Mixture **A** was added to the reaction vessel, and the reaction was heated at 160 °C for 30 min. The reaction was followed with radio-HPLC.

*Synthesis of [^{18}F]**4** for Preclinical Studies.* Aqueous [^{18}F]F^- was trapped in a PS-HCO_3^- anion exchange cartridge (Synthra GmbH) preconditioned with potassium oxalate (3 mL, 10 mg/mL) and water (2 mL). The cartridge was washed with 1 mL CH_3CN, and [^{18}F]F^- was eluted to a conical vial with the mixture **A** as described above. The cartridge was rinsed with DMSO (150 μL) and 1:1 DMSO/MeCN solution (50 μL). This mixture was heated at 160 °C for 30 min. After heating, the mixture was diluted with HPLC eluent (1 mL) and purified by semipreparative HPLC. The product fraction was collected, diluted with water (20 mL), and loaded on a C18 Plus Light Sep-Pak cartridge (Waters corp, Milford, Massachusetts) preconditioned with ethanol (7 mL) and water (10 mL). The cartridge was washed with water (20 mL), and the product was eluted with ethanol (300 μL) followed by 9 mg/mL NaCl (aq) (2.7 mL).

For quality control, pH was measured with pH strips and radiochemical purity was determined with analytical radio-HPLC. The identity was confirmed with FPATPP reference standard **4**.

Synthesis of [^{18}F]FMPEP-d_2. [^{18}F]FMPEP-d_2 was synthesized as previously reported.[32]

Animals. *Experimental Animals.* Experiments with animals ([^{18}F]**4**, n = 17; [^{18}F]FMPEP-d_2, n = 19) were conducted under the guidelines of the International Council of Laboratory Animal Science (ICLAS). This study was approved by the Finnish National Animal Experiment Board (ESAVI/16273/2019 and ESAVI/4660/04.10.07/2016). Experimental animals were housed at the Central Animal Laboratory of the University of Turku under standardized conditions (temperature 21 °C, humidity 55% ± 5%, lights on from 7:00 a.m. to 7:00 p.m.), with free access to certified standard laboratory soy-free chow (RM3 soya-free, 801710, Special Diets Service) and tap water. Studies with [^{18}F]**4** were conducted with healthy wild-type 2 (n = 11, males, weight 25.5 ± 1.3 g) and 4 to 5 month old (n = 6, 2 females, weight 32.1 ± 4.2 g) C57BL/6NRj mice (Charles River Laboratories, Research Models and Services, Germany). The *ex vivo* biodistribution study with [^{18}F]FMPEP-d_2 was conducted with healthy wild-type 3−4 month old (n = 7, males, weight 32.8 ± 4.6 g) and 1.5−6 month old (n = 12, 5 females, weight 26.5 ± 6.6 g) C57BL/6N mice. The injected volume of the tracer was 155 ± 42 μL.

*In Vivo PET Imaging with [^{18}F]**4**.* Dynamic PET scans were performed for 5 month old mice with an Inveon Multimodality PET/CT scanner (Siemens Medical Solutions USA, Knoxville, Tennessee). Mice were anesthetized with 2.5% isoflurane/oxygen gas, and body temperature was maintained with a heating pad and a bubble-wrap cover. CT transmission scans were performed to correct for attenuation. PET scans were initiated in parallel with an intravenous (iv) bolus injection of [^{18}F]**4** to the mouse tail vein (4−5 month old, n = 6, 2 females; injected radioactivity 4.0 ± 0.4 MBq; injected mass 56 ± 25 ng, 1.7 ± 0.7 μg/kg).

Dynamic emission scans were acquired for 120 min in 3D list mode, with an energy window of 350−650 keV. Scanning times were 120 min (54 frames 30 × 10 s, 15 × 60 s, 4 × 300 s, 2 × 600 s, 3 × 1200 s). The list mode data were stored in 3D sinograms. Data were reconstructed with OSEM3D/MAP software (2 OSEM3D iterations and 18 MAP iterations). The PET/CT images were preprocessed in Matlab R2017a (The MathWorks, Natick, Massachusetts) with an in-house semiautomated pipeline for preclinical images that uses SPM12 (Wellcome Department of Cognitive Neurology, London, UK) preprocessing functionalities and analysis routines. Images were first cropped to a bounding box containing the heads, and individual PET images were coregistered through a rigid-body transformation to their corresponding CT scan. Subjects were spatially normalized through a two-step registration (a rigid followed by an affine transformation) of each subject's CT to a template CT that was previously constructed as an average of several subjects and was aligned with an atlas T2-weighted MRI template. The combination of transformations was then applied to the PET images, which were also resampled to a voxel size of 0.2 × 0.2 × 0.2 mm^3 (trilinear interpolation), matching the anatomical atlas dimensions.

Volume of interest (VOI) analysis of the whole brain, neocortex, and hippocampus was performed on each subject by averaging the signal inside a slightly modified version of the Ma et al.[40] atlas delineated VOIs, and data were obtained as standardized uptake values (SUVs). SUVs were calculated as follows: SUV = tissue activity concentration (Bq/mL)/(injected dose (Bq)/body weight (g)); it was assumed that 1 mL of tissue equals 1 g. Tissue activity and dose were decay corrected to the same time point.

*Ex Vivo Biodistribution and Brain Autoradiography with [^{18}F]**4**.* All *in vivo* animals (n = 6, 2 females) and additional 2 month old mice (n = 11, males, injected radioactivity 7.0 ± 3.0 MBq; injected mass 160 ± 60 ng, 6.2 ± 2.6 μg/kg) were used for *ex vivo* studies to examine the biodistribution and metabolism of [^{18}F]**4**. Thus, the injected dose and injected mass to all the animals used (n = 17) were 5.9 ± 2.8 MBq and 120 ± 70 ng, 4.6 ± 3.0 μg/kg, respectively. After iv injection of [^{18}F]**4**, mice were sacrificed in deep anesthesia of 4.0% isoflurane with cardiac puncture at 30 (n = 4), 60 (n = 2), and 120 min (*in vivo* animals, n = 6 and 2 month old mice n = 5). Organs were immediately dissected, weighed, and measured for ^{18}F-radioactivity in a 2480 Wizard Gamma Counter (Wallac PerkinElmer, Turku, Finland).

For autoradiography, brains were further frozen and cut into 20 μm coronal cryosections for digital autoradiography, and the slices were exposed on an imaging plate (BAS-TR2025, Fuji Photo Film Co.) for approximately 2 half-lives and scanned with a Fuji BAS5000 phosphorimager (FUJIFILM Life Science, Stamford, Connecticut). Digital autoradiographic images were analyzed for count densities with the Aida 4 program (Raytest Isotopenmessgeräte GmbH, Straubenhardt, Germany). For brain slices, regions of interest (ROIs) were drawn over the parietotemporal cortex, striatum, frontal cortex, hippocampus, cerebellar gray matter, and thalamus. The autoradiography was quantified as ratios of the different ROIs relative to the thalamus, which was used as the reference region.

https://dx.doi.org/10.1021/acschemneuro.0c00313
ACS Chem. Neurosci. 2020, 11, 2009−2018

Ex Vivo Biodistribution with [^{18}F]FMPEP-d_2. After iv injection of [^{18}F]FMPEP-d_2 to the mouse tail vein, the mice were sacrificed at the following time points: 30 min (3−4 month old, n = 3, males; injected radioactivity 1.3 ± 0.3 MBq; injected mass 1.5 ± 0.5 ng), 60 min (3−4 months old, n = 4, males; injected radioactivity 1.2 ± 0.8 MBq; injected mass 1.3 ± 1.0 ng), and 120 min (1.5−6 month old, n = 12, 5 females; injected radioactivity 2.6 ± 0.8 MBq; injected mass 3.1 ± 1.1 ng). Mice were sacrificed in deep anesthesia of 4.0% isoflurane with cardiac puncture. Organs were operated in the similar manner as in the biodistribution study with [^{18}F]**4**.

*Pretreatment Studies with [^{18}F]**4**.* The specificity of [^{18}F]**4** on mouse cerebral CB1Rs was examined in a 120 min *in vivo* study, and then, the same mice were used for *ex vivo* biodistribution and brain autoradiography studies. An inverse CB1R agonist rimonabant (90 μL, 2 mg/kg in 10% EtOH in Kleptose β-cyclodextrin; rimonabant, Merck; Kleptose β-cyclodextrin, APL pharma specials, Stockholm, Sweden) was administered iv into the mouse tail vein (n = 3, 1 female) 10 min prior to injection of [^{18}F]**4**. Control mice (n = 3, 1 female) were the given vehicle (90 μL, 10% EtOH in Kleptose β-cyclodextrin). The binding specificity of [^{18}F]**4** was estimated by comparing the binding of [^{18}F]**4** in the presence and absence of rimonabant. Mice were sacrificed 120 min after iv injection of [^{18}F]**4**, and the ^{18}F-radioactivity distribution differences between pretreated and control mice were examined with *in vivo* PET imaging, *ex vivo* autoradiography, and 2480 Wizard Gamma Counter, and the data were analyzed as described in the previous sections.

*Metabolite Analyses with [^{18}F]**4**.* The 2 month old animals (n = 11, used only for *ex vivo* studies) were used for metabolite analysis. Plasma and brain samples were collected at 30 (n = 4), 60 (n = 2), and 120 min (n = 5) p.i. Plasma samples were treated with MeCN and centrifuged to remove the proteins from the solution. Brain tissue samples were treated with the 40/60 (v/v) 1% TFA (aq)/MeCN solution and then centrifuged. The supernatants were applied to HPTLC silica gel 60 RP-18 plates (Art. 1.05914.0001, Merck, Darmstadt, Germany), and the plates were developed in 40/60 (v/v) 1% TFA (aq)/ MeCN. After drying, the TLC plates were exposed to an imaging plate for approximately 4 h and the imaging plate was scanned with a Fuji Analyzer BAS5000. The amount of [^{18}F]**4** and its radioactive metabolites were analyzed with the Aida 4 program, and the curves were fitted with GraphPad Prism 6.0 (GraphPad Software, San Diego, California) using a double exponential decay equation.

Statistical Analyses. Values are expressed as mean ± standard deviation (SD). For *ex vivo* brain autoradiography and biodistribution, statistical analyses were performed with the Mann−Whitney U test (GraphPad Prism 6.0).

AUTHOR INFORMATION

Corresponding Author

Anna K. Kirjavainen − *Radiopharmaceutical Chemistry Laboratory, Turku PET Centre, University of Turku, Turku, Finland*; Email: anna.kirjavainen@utu.fi

Authors

Salla Lahdenpohja − *Radiopharmaceutical Chemistry Laboratory, Turku PET Centre, University of Turku, Turku, Finland*; orcid.org/0000-0003-2456-5009

Noora A. Rajala − *Radiopharmaceutical Chemistry Laboratory, Turku PET Centre, University of Turku, Turku, Finland*

Jatta S. Helin − *Preclinical Imaging, Turku PET Centre and MediCity Research Laboratory, University of Turku, Turku, Finland*

Merja Haaparanta-Solin − *Preclinical Imaging, Turku PET Centre and MediCity Research Laboratory, University of Turku, Turku, Finland*

Olof Solin − *Radiopharmaceutical Chemistry Laboratory, Turku PET Centre and Department of Chemistry, University of Turku, Turku, Finland; Accelerator Laboratory, Åbo Akademi University, Turku, Finland*

Francisco R. López-Picón − *Preclinical Imaging, Turku PET Centre and MediCity Research Laboratory, University of Turku, Turku, Finland*

Complete contact information is available at: https://pubs.acs.org/10.1021/acschemneuro.0c00313

Author Contributions

▲S.L. and N.A.R. contributed equally. All authors have given approval to the final version of the manuscript.

Funding

The study was funded by the Academy of Finland (grants no. 266891 and 307924) and State Funding for University Level Health Research (project no. 11017).

Notes

The authors declare no competing financial interest.

ACKNOWLEDGMENTS

We acknowledge the cyclotron staff at Åbo Akademi University and preclinical imaging staff at University of Turku for their technical help. The Central Animal Laboratory of University of Turku is acknowledged for the animal care.

ABBREVIATIONS

A_m, molar activity; Bl., blocked; CB_1 receptor, CB1R, cannabinoid receptor 1; CB2R, cannabinoid receptor 2; CB, cortex and cerebellar gray matter; CT, computed tomography; Fc, frontal cortex; Gp, globus pallidus; GPCR, G protein-coupled receptor; Hippo, hippocampus; HPLC, high performance liquid chromatography; %ID/g, injected dose per gram of tissue; iv, intravenous; PET, positron emission tomography; p.i., post injection; Ptc, parietotemporal cortex; ROI, region of interest; SD, standard deviation; SPE, solid-phase extraction; SUV, standardized uptake value; Str, striatum; Tha, thalamus; TLC, thin-layer chromatography; VOI, volume of interest

REFERENCES

(1) Howlett, A. C., Barth, F., Bonner, T. I., Cabral, G., Casellas, P., Devane, W. A., Felder, C. C., Herkenham, M., Mackie, K., Martin, B. R., Mechoulam, R., and Pertwee, R. G. (2002) International Union of Pharmacology. XXVII. Classification of Cannabinoid Receptors. *Pharmacol Rev. 54* (2), 161−202.

(2) Mechoulam, R., and Parker, L. A. (2013) The Endocannabinoid System and the Brain. *Annu. Rev. Psychol. 64*, 21−47.

(3) Herkenham, M., Lynn, A. B., Little, M. D., Johnson, M. R., Melvin, L. S., de Costa, B. R., and Rice, K. C. (1990) Cannabinoid Receptor Localization in Brain. *Proc. Natl. Acad. Sci. U. S. A. 87* (5), 1932−1936.

(4) Glass, M., Dragunow, M., and Faull, R. L. (1997) Cannabinoid Receptors in the Human Brain: A Detailed Anatomical and Quantitative Autoradiographic Study in the Fetal, Neonatal and Adult Human Brain. *Neuroscience 77* (2), 299−318.

(5) Jordan, C. J., and Xi, Z.-X. (2019) Progress in Brain Cannabinoid CB_2 Receptor Research: From Genes to Behavior. *Neurosci. Biobehav. Rev. 98*, 208−220.

(6) Yu, S.-J., Reiner, D., Shen, H., Wu, K.-J., Liu, Q.-R., and Wang, Y. (2015) Time-Dependent Protection of CB_2 Receptor Agonist in Stroke. *PLoS One 10* (7), e0132487.

(7) Fattore, L. (2015) *Cannabinoids in Neurologic and Mental Disease*, Elsevier Inc., San Diego, CA. .

(8) Fagan, S. G., and Campbell, V. A. (2015) Endocannabinoids and Alzheimer's Disease. In *Cannabinoids in Neurologic and Mental Disease* (Fattore, L., Ed.) pp 15−33, Elsevier Inc, San Diego, CA.

(9) Yasuno, F., Brown, A. K., Zoghbi, S. S., Krushinski, J. H., Chernet, E., Tauscher, J., Schaus, J. M., Phebus, L. A., Chesterfield, A.

K., Felder, C. C., Gladding, R. L., Hong, J., Halldin, C., Pike, V. W., and Innis, R. B. (2008) The PET Radioligand [^{11}C]MePPEP Binds Reversibly and with High Specific Signal to Cannabinoid CB_1 Receptors in Nonhuman Primate Brain. *Neuropsychopharmacology 33* (2), 259−269.

(10) Donohue, S. R., Krushinski, J. H., Pike, V. W., Chernet, E., Phebus, L., Chesterfield, A. K., Felder, C. C., Halldin, C., and Schaus, J. M. (2008) Synthesis, *Ex Vivo* Evaluation, and Radiolabeling of Potent 1,5-Diphenylpyrrolidin-2-One Cannabinoid Subtype-1 Receptor Ligands as Candidates for *in Vivo* Imaging. *J. Med. Chem. 51* (18), 5833−5842.

(11) Casteels, C., Koole, M., Celen, S., Bormans, G., and Van Laere, K. (2012) Preclinical Evaluation and Quantification of [^{18}F]MK-9470 as a Radioligand for PET Imaging of the Type 1 Cannabinoid Receptor in Rat Brain. *Eur. J. Nucl. Med. Mol. Imaging 39* (9), 1467−1477.

(12) Burns, H. D., Van Laere, K., Sanabria-Bohorquez, S., Hamill, T. G., Bormans, G., Eng, W.-s., Gibson, R., Ryan, C., Connolly, B., Patel, S., Krause, S., Vanko, A., Van Hecken, A., Dupont, P., De Lepeleire, I., Rothenberg, P., Stoch, S. A., Cote, J., Hagmann, W. K., Jewell, J. P., Lin, L. S., Liu, P., Goulet, M. T., Gottesdiener, K., Wagner, J. A., de Hoon, J., Mortelmans, L., Fong, T. M., and Hargreaves, R. J. (2007) [^{18}F]MK-9470, a Positron Emission Tomography (PET) Tracer for in Vivo Human PET Brain Imaging of the Cannabinoid-1 Receptor. *Proc. Natl. Acad. Sci. U. S. A. 104* (23), 9800−9805.

(13) Preshlock, S., Tredwell, M., and Gouverneur, V. (2016) ^{18}F-Labeling of Arenes and Heteroarenes for Applications in Positron Emission Tomography. *Chem. Rev. 116* (2), 719−766.

(14) Brooks, A. F., Topczewski, J. J., Ichiishi, N., Sanford, M. S., and Scott, P. J. H. (2014) Late-Stage [^{18}F]Fluorination: New Solutions to Old Problems. *Chem. Sci. 5* (12), 4545−4553.

(15) Deng, X., Rong, J., Wang, L., Vasdev, N., Zhang, L., Josephson, L., and Liang, S. H. (2019) Chemistry for Positron Emission Tomography: Recent Advances in ^{11}C-, ^{18}F-, ^{13}N-, and ^{15}O-Labeling Reactions. *Angew. Chem., Int. Ed. 58* (9), 2580−2605.

(16) Edem, P. E., Steen, E. J. L., Kjær, A., and Herth, M. M. (2019) Fluorine-18 Radiolabeling Strategies—Advantages and Disadvantages of Currently Applied Labeling Methods. In *Late-Stage Fluorination of Bioactive Molecules and Biologically-Relevant Substrates* (Postigo, A., Ed.) pp 29−103, Elsevier, United States.

(17) Reddy, V. P. (2020) Synthesis and Applications of ^{18}F-Labeled Compounds. In *Organofluorine Chemistry* (Reddy, V. P., Ed.) pp 215−278, Elsevier, United States.

(18) Pike, V. W., and Aigbirhio, F. I. (1995) Reactions of Cyclotron-Produced [^{18}F]Fluoride with Diaryliodonium Salts—a Novel Single-Step Route to No-Carrier-Added [^{18}F]Fluoroarenes. *J. Chem. Soc., Chem. Commun. 1995* (21), 2215−2216.

(19) Mu, L., Fischer, C. R., Holland, J. P., Becaud, J., Schubiger, P. A., Schibli, R., Ametamey, S. M., Graham, K., Stellfeld, T., Dinkelborg, L. M., and Lehmann, L. (2012) ^{18}F-Radiolabeling of Aromatic Compounds Using Triarylsulfonium Salts. *Eur. J. Org. Chem. 2012* (5), 889−892.

(20) Cardinale, J., Ermert, J., Humpert, S., and Coenen, H. H. (2014) Iodonium Ylides for One-Step, No-Carrier-Added Radiofluorination of Electron Rich Arenes, Exemplified with 4-(([^{18}F]-Fluorophenoxy)-Phenylmethyl)Piperidine NET and SERT Ligands. *RSC Adv. 4*, 17293−17299.

(21) Lee, E., Kamlet, A. S., Powers, D. C., Neumann, C. N., Boursalian, G. B., Furuya, T., Choi, D. C., Hooker, J. M., and Ritter, T. (2011) A Fluoride-Derived Electrophilic Late-Stage Fluorination Reagent for PET Imaging. *Science (Washington, DC, U. S.) 334* (6056), 639−642.

(22) Lee, E., Hooker, J. M., and Ritter, T. (2012) Nickel-Mediated Oxidative Fluorination for PET with Aqueous [^{18}F]Fluoride. *J. Am. Chem. Soc. 134* (42), 17456−17458.

(23) Tredwell, M., Preshlock, S. M., Taylor, N. J., Gruber, S., Huiban, M., Passchier, J., Mercier, J., Génicot, C., and Gouverneur, V. (2014) A General Copper-mediated Nucleophilic ^{18}F-Fluorination of Arenes. *Angew. Chem., Int. Ed. 53* (30), 7751−7755.

(24) Mossine, A. V., Brooks, A. F., Makaravage, K. J., Miller, J. M., Ichiishi, N., Sanford, M. S., and Scott, P. J. H. (2015) Synthesis of [^{18}F]Arenes via the Copper-Mediated [^{18}F]Fluorination of Boronic Acids. *Org. Lett. 17* (23), 5780−5783.

(25) Makaravage, K. J., Brooks, A. F., Mossine, A. V., Sanford, M. S., and Scott, P. J. H. (2016) Copper-Mediated Radiofluorination of Arylstannanes with [^{18}F]KF. *Org. Lett. 18* (20), 5440−5443.

(26) Beyzavi, M. H., Mandal, D., Strebl, M. G., Neumann, C. N., D'Amato, E. M., Chen, J., Hooker, J. M., and Ritter, T. (2017) ^{18}F-Deoxyfluorination of Phenols via Ru π-Complexes. *ACS Cent. Sci. 3* (9), 944−948.

(27) Rickmeier, J., and Ritter, T. (2018) Site-Specific Deoxyfluorination of Small Peptides with [^{18}F]Fluoride. *Angew. Chem., Int. Ed. 57* (43), 14207−14211.

(28) Borgan, F., Laurikainen, H., Veronese, M., Marques, T. R., Haaparanta-Solin, M., Solin, O., Dahoun, T., Rogdaki, M., Salokangas, R. K., Karukivi, M., Di Forti, M., Turkheimer, F., Hietala, J., and Howes, O. (2019) In Vivo Availability of Cannabinoid 1 Receptor Levels in Patients with First-Episode Psychosis. *JAMA Psychiatry 76* (10), 1074−1084.

(29) Laurikainen, H., Tuominen, L., Tikka, M., Merisaari, H., Armio, R.-L., Sormunen, E., Borgan, F., Veronese, M., Howes, O., Haaparanta-Solin, M., Solin, O., and Hietala, J. (2019) Sex Difference in Brain CB_1 Receptor Availability in Man. *NeuroImage 184*, 834−842.

(30) Lahesmaa, M., Eriksson, O., Gnad, T., Oikonen, V., Bucci, M., Hirvonen, J., Koskensalo, K., Teuho, J., Niemi, T., Taittonen, M., Lahdenpohja, S., Din, M. U., Haaparanta-Solin, M., Pfeifer, A., Virtanen, K. A., and Nuutila, P. (2018) Cannabinoid Type 1 Receptors Are Upregulated during Acute Activation of Brown Adipose Tissue. *Diabetes 67* (7), 1226−1236.

(31) Takkinen, J. S., López-Picón, F. R., Kirjavainen, A. K., Pihlaja, R., Snellman, A., Ishizu, T., Löyttyniemi, E., Solin, O., Rinne, J. O., and Haaparanta-Solin, M. (2018) [^{18}F]FMPEP-d_2 PET Imaging Shows Age- and Genotype-Dependent Impairments in the Availability of Cannabinoid Receptor 1 in a Mouse Model of Alzheimer's Disease. *Neurobiol. Aging 69*, 199−208.

(32) Lahdenpohja, S., Keller, T., Forsback, S., Viljanen, T., Kokkomäki, E., Kivelä, R. V., Bergman, J., Solin, O., and Kirjavainen, A. K. (2020) Automated GMP Production and Long-Term Experience in Radiosynthesis of CB_1 Tracer [^{18}F]FMPEP-d_2. *J. Labelled Compd. Radiopharm.*, 1.

(33) The International Council for Harmonisation of Technical Requirements for Pharmaceuticals for Human Use (ICH): Guideline for Elemental Impurities Q3D(R1), 2019.

(34) Rinaldi-Carmona, M., Barth, F., Heaulme, M., Shire, D., Calandra, B., Congy, C., Martinez, S., Maruani, J., Neliat, G., Caput, D., Ferrara, P., Soubrie, P., Breliere, J. C., and Le Fur, G. (1994) SR141716A, a Potent and Selective Antagonist of the Brain Cannabinoid Receptor. *FEBS Lett. 350* (2−3), 240−244.

(35) Terry, G. E., Hirvonen, J., Liow, J.-S., Zoghbi, S. S., Gladding, R., Tauscher, J. T., Schaus, J. M., Phebus, L., Felder, C. C., Morse, C. L., Donohue, S. R., Pike, V. W., Halldin, C., and Innis, R. B. (2010) Imaging and Quantitation of Cannabinoid CB_1 Receptors in Human and Monkey Brains Using ^{18}F-Labeled Inverse Agonist Radioligands. *J. Nucl. Med. 51* (1), 112−120.

(36) Van Laere, K., Goffin, K., Casteels, C., Dupont, P., Mortelmans, L., de Hoon, J., and Bormans, G. (2008) Gender-Dependent Increases with Healthy Aging of the Human Cerebral Cannabinoid-Type 1 Receptor Binding Using [^{18}F]MK-9470 PET. *NeuroImage 39* (4), 1533−1541.

(37) Ruehle, S., Remmers, F., Romo-Parra, H., Massa, F., Wickert, M., Wörtge, S., Häring, M., Kaiser, N., Marsicano, G., Pape, H.-C., and Lutz, B. (2013) Cannabinoid CB1 Receptor in Dorsal Telencephalic Glutamatergic Neurons: Distinctive Sufficiency for Hippocampus-Dependent and Amygdala-Dependent Synaptic and Behavioral Functions. *J. Neurosci. 33* (25), 10264−10277.

(38) Remmers, F., Lange, M. D., Hamann, M., Ruehle, S., Pape, H.-C., and Lutz, B. (2017) Addressing Sufficiency of the CB_1 Receptor

https://dx.doi.org/10.1021/acschemneuro.0c00313
ACS Chem. Neurosci. 2020, 11, 2009−2018

for Endocannabinoid-Mediated Functions through Conditional Genetic Rescue in Forebrain GABAergic Neurons. *Brain Struct. Funct. 222* (8), 3431−3452.
(39) Laurén, H. B., Lopez-Picon, F., Brandt, A. M., Rios-Rojas, C., and Holopainen, I. E. (2010) Transcriptome Analysis of the Hippocampal CA1 Pyramidal Cell Region after Kainic Acid-Induced Status Epilepticus in Juvenile Rats. *PLoS One 5* (5), No. e10733.
(40) Ma, Y., Smith, D., Hof, P., Foerster, B., Hamilton, S., Blackband, S., Yu, M., and Benveniste, H. (2008) *In Vivo* 3D Digital Atlas Database of the Adult C57BL/6J Mouse Brain by Magnetic Resonance Microscopy. *Front. Neuroanat. 2*, 1.

https://dx.doi.org/10.1021/acschemneuro.0c00313
ACS Chem. Neurosci. 2020, 11, 2009−2018